PHASE NOISE EFFECTS ON SIGNAL DETECTION FOR UWB/WIMAX COEXISTENCE

Sanghoon Park, Lawrence E. Larson, and Laurence B. Milstein
Center for Wireless Communication, Dept. of Electrical and Computer Engineering
University of California - San Diego, La Jolla, CA 92037

ABSTRACT

The effect of local oscillator (LO) phase noise of an ultra-wide band (UWB) receiver on the detection of a nearby WiMAX receiver is investigated. An expression for the spectrum broadening effect due to the phase noise is derived, and a practical method is presented to estimate the in-band interference due to the phase noise interaction with an interfering adjacent channel signal.

INTRODUCTION

After the Federal Communications Commission (FCC) authorized the unlicensed use of the frequency band between 3.1 to 10.6 GHz for UWB communication systems [1], interference problems became a concern. One of the systems that share the frequency spectrum with UWB is the worldwide interoperability for microwave access (WiMAX) system. Based on the IEEE 802.16 standard, WiMAX is currently utilizing several frequency bands below 11 GHz, such as the unlicensed 5 GHz band, the licensed 3.5 GHz band, and the licensed 2.5 GHz band [2]. Since the WiMAX system is expected to share the frequency spectrum with UWB, an active WiMAX device detection scheme is highly desirable for UWB devices.

Detecting WiMAX downlink signal is a possible approach, but it has the drawback that it will confine the available frequency spectrum for the UWB device even when no WiMAX receiver is present. As shown in Figure 1, the radius of the UWB system is confined to about 10 m, and so detecting the LO leakage signal from a nearby WiMAX mobile terminal receiver could be used by a UWB device to detect the presence of that WiMAX receiver [3]. However, the detection sensitivity is of major concern due to the very low level of the incoming leakage signal power. In particular, the phase noise of the UWB detector's RF oscillator can degrade the overall detection sensitivity due to the spectrum broadening effect.

In this paper, we evaluate the effect of receiver phase noise on the in-band interference in an additive white Gaussian noise (AWGN) environment and apply the result to the detection of a WiMAX mobile terminal (MT) by a UWB device.

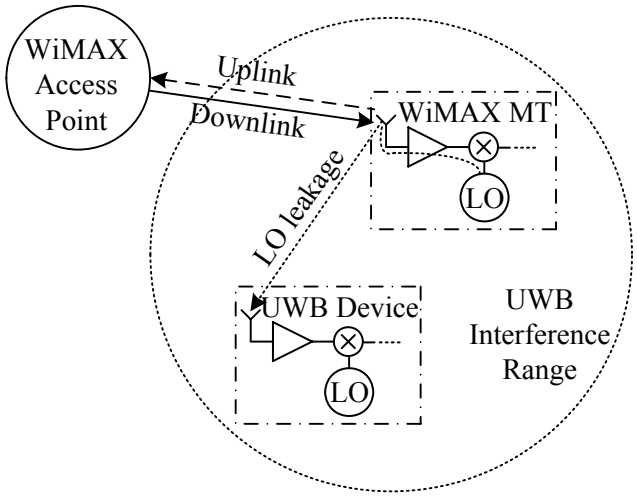

Figure 1. Coexistence situation where a WiMAX MT is inside the UWB interference range.

SIGNAL DETECTION FOR UWB/WIMAX COEXISTENCE

When a WiMAX MT is in the receive mode, a small portion of the receiver LO signal power leaks to the antenna and radiates as shown in Figure 1. Typically, a leakage signal power level of –70 to –90 dBm is expected at the antenna port [4]. This signal is received at the UWB antenna, and is either

$$r(t) = n_W(t) \tag{1}$$

or

$$r(t) = s(t) + n_W(t) \tag{2}$$

where $s(t)$ and $n_W(t)$ denote the received leakage signal from the WiMAX MT and the received noise, respectively.

We assume that a UWB device relies on a Discrete Fourier Transform (DFT) to discriminate the unmodulated leakage signal from the background noise. The UWB device determines that $s(t)$ is absent if the magnitude

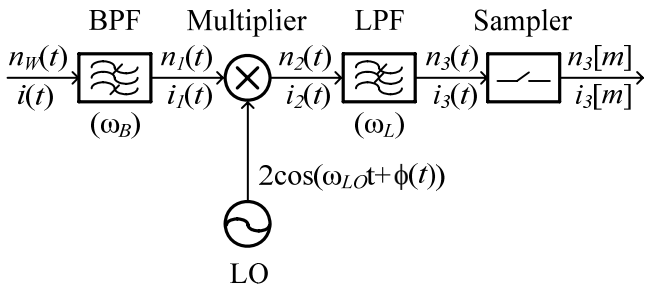

Figure 2. Simplified receiver architecture. $n_W(t)$ and $i(t)$ are noise and an interfering adjacent channel signal, respectively.

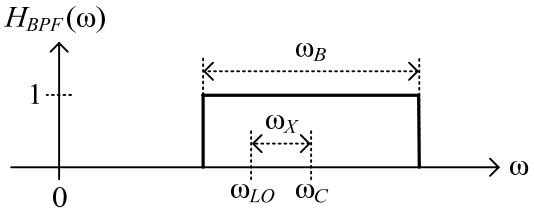

Figure 3. Frequency response of the BPF. ω_C is the center frequency of the BPF. ω_X is the frequency difference between ω_{LO} and ω_C.

response of all the DFT frequency bins fall below a specified threshold. If at least one of the DFT outputs exceeds the threshold, the receiver determines that $s(t)$ is present. The detection performance can be described by the probabilities of false alarm (P_{FA}) and missed detection (P_{MD}).

SPECTRUM BROADENING EFFECT DUE TO PHASE NOISE

A simplified block diagram of a direct conversion type receiver is shown in Figure 2. Denoting the phase noise by $\phi(t)$, and assuming that the standard deviation of $\phi(t)$ is much less than one radian, the LO signal can be described by

$$\begin{aligned} LO(t) &= 2\cos\left(\omega_{LO}t+\phi(t)\right) \\ &\approx 2\cos\left(\omega_{LO}t\right)-2\phi(t)\sin\left(\omega_{LO}t\right). \end{aligned} \tag{3}$$

The frequency response of the front-end bandpass filter (BPF) is shown in Figure 3. It is assumed that the bandwidth of the BPF (ω_B) is wide enough to accommodate the WiMAX system. After the BPF, the

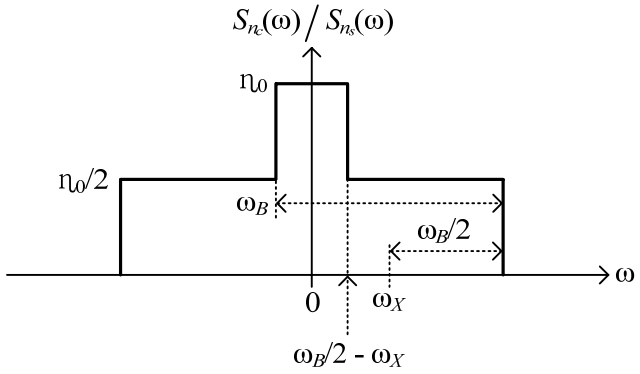

Figure 4. Power spectral density of the in-phase and quadrature components of $n_I(t)$.

bandpass noise $n_1(t)$ is described by

$$n_1(t) = n_C(t)\cos\left(\omega_{LO}t+\theta_1\right) - n_S(t)\sin\left(\omega_{LO}t+\theta_1\right) \tag{4}$$

where θ_1, $n_C(t)$, and $n_S(t)$ denote an arbitrary phase, the inphase component, and the quadrature component of $n_1(t)$, respectively. Since $n_W(t)$ is a zero-mean Gaussian random process, $n_C(t)$ and $n_S(t)$ are also both zero-mean Gaussian random processes, and the power spectral density (PSD) of $n_C(t)$ is given by

$$S_{n_C}(\omega) = \frac{\eta_0}{2}\left[P_{\omega_B/2}\left(\omega+\omega_X\right)+P_{\omega_B/2}\left(\omega-\omega_X\right)\right] \tag{5}$$

where η_0 is the single-sided PSD of the AWGN [5], and $P_a(x)$ is the pulse function defined by

$$P_a(x) \triangleq \begin{cases} 1, & -a \le x \le a \\ 0, & otherwise. \end{cases} \tag{6}$$

As is well known, $n_S(t)$ has identical statistics to $n_C(t)$. Figure 4 shows $S_{n_C}(\omega)$ or $S_{n_S}(\omega)$.

Denoting the impulse response of the lowpass filter (LPF) by $h_L(t)$, the output of the LPF is given by

$$n_3(t) = \left[n_A(t)+\phi(t)n_B(t)\right] * h_L(t) \tag{7}$$

where

$$n_A(t) = n_C(t)\cos\theta_1 - n_S(t)\sin\theta_1 \tag{8}$$

and

$$n_B(t) = n_C(t)\sin\theta_1 + n_S(t)\cos\theta_1. \tag{9}$$

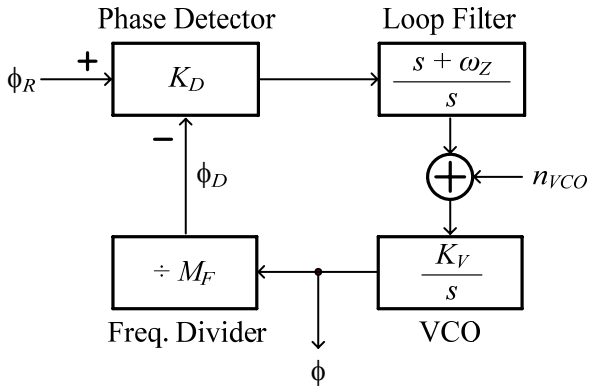

Figure 5. Phase-domain model of the PLL. n_{VCO} denotes the input-referred voltage-controlled oscillator (VCO) noise. ϕ and ϕ_R represent the excess phase of the LO and reference signal, respectively.

We assume that ω_{LO} is sufficiently large so that the double frequency terms after the multiplier are filtered out by the LPF. Note that $n_A(t)$ and $n_B(t)$ are also zero-mean Gaussian random processes. Since the autocorrelations of both $n_A(t)$ and $n_B(t)$ are identical to that of $n_C(t)$, the PSD of either $n_A(t)$ or $n_B(t)$ is given by (5).

In (7), we define $n_\phi(t)$ as follows:

$$n_\phi(t) \triangleq \phi(t) n_B(t). \tag{10}$$

Since $\phi(t)$ and $n_B(t)$ are independent, the PSD of $n_\phi(t)$ is given by

$$S_{n_\phi}(\omega) = S_\phi(\omega) * S_{n_B}(\omega). \tag{11}$$

In order for the LO signal to achieve a precise frequency, a phase-locked loop (PLL) is widely used. Figure 5 shows the LTI phase-domain model of a typical charge-pump PLL in the locked condition. Since the excess phase of the reference signal is small [6], [7], it is assumed that the phase noise of the LO is dominated by $n_{VCO}(t)$. From Figure 5,

$$\phi(s) = \frac{sK_V}{s^2 + 2\varsigma_0\omega_0 s + \omega_0^2} n_{VCO}(s) \tag{12}$$

where

$$\omega_0 = \sqrt{\frac{K_D K_V \omega_z}{M_F}} \tag{13}$$

and

$$\varsigma_0 = \frac{1}{2}\sqrt{\frac{K_D K_V}{M_F \omega_z}}. \tag{14}$$

Since the quantity ς_0 is typically close to unity, the double-sided PSD of $\phi(t)$ is given by

$$S_\phi(\omega) \approx \frac{\omega^2 K_V^2}{\left(\omega^2 + \omega_0^2\right)^2}\left(\frac{\eta_{VCO}}{2}\right) \tag{15}$$

where η_{VCO} and K_V denote the single-sided PSD of $n_{VCO}(t)$ and the frequency gain of the VCO, respectively. It is noted that the phase noise spectrum is often described by the relative power ratio around the fundamental oscillation frequency, f_{LO} [8]. This can be expressed as

$$\mathfrak{L}(f) = \frac{S_{LO}(f_{LO}+f)}{P_{LO}/2} \tag{16}$$

where $S_{LO}(f)$ and P_{LO} denote the PSD and power of the LO signal, respectively. For the case of interest [9], [10] $\mathfrak{L}(f) = S_\phi(f)$. From (15), at a given frequency offset, f, that is greater than f_0, $\mathfrak{L}(f)$ can be approximated by

$$\mathfrak{L}(f) \approx \frac{1}{f^2}\left(\frac{K_V^2 \eta_{VCO}}{8\pi^2}\right) \tag{17}$$

Using (9) and (15) in (11), $S_{n_\phi}(\omega)$ is given by

$$\begin{aligned} S_{n_\phi}(\omega) = \frac{\eta_0 \eta_{VCO} K_V^2}{16\pi\omega_0}\big[& V(\omega+\omega_B/2+\omega_X) \\ & - V(\omega-\omega_B/2+\omega_X) + V(\omega+\omega_B/2-\omega_X) \\ & - V(\omega-\omega_B/2-\omega_X) - W(\omega+\omega_B/2+\omega_X) \\ & + W(\omega-\omega_B/2+\omega_X) - W(\omega+\omega_B/2-\omega_X) \\ & + W(\omega-\omega_B/2-\omega_X)\big] \end{aligned} \tag{18}$$

where

$$V(x) \triangleq \tan^{-1}\left(x/\omega_0\right) \tag{19}$$

and

$$W(x) \triangleq \frac{1}{2}\sin\left[2\tan^{-1}\left(x/\omega_0\right)\right]. \tag{20}$$

Due to the convolution of $S_{n_B}(\omega)$ with $S_\phi(\omega)$, the bandwidth of $n_\phi(t)$ is wider than that of $n_B(t)$. Therefore, the presence of the phase noise causes the energy of the multiplier input signal to spill over in other signal spectral

bands. This in-band interference can be a serious problem when a strong out-of-band signal is present.

PHASE NOISE INTERACTION WITH AN ADJACENT CHANNEL SIGNAL

The spectrum broadening effect can introduce in-band interference from an out-of-band signal. Suppose that the UWB detector is searching a particular channel of the WiMAX system, while an adjacent WiMAX channel is concurrently occupied. The received interfering adjacent channel signal is given by

$$\begin{aligned} i(t) = i_C(t)\cos\left(\left[\omega_{LO}+\omega_{ch}\right]t+\theta_i\right) \\ - i_S(t)\sin\left(\left[\omega_{LO}+\omega_{ch}\right]t+\theta_i\right) \end{aligned} \tag{21}$$

where θ_i, $i_C(t)$, $i_S(t)$, and ω_{ch} denote an arbitrary phase, the inphase component, the quadrature component, and the bandwidth, respectively, of the received WiMAX signal. Both $i_C(t)$ and $i_S(t)$ can be modeled as independent, identical, WSS bandpass Gaussian processes [11], [12]. Since the OFDM signal consists of a large number of sub-carriers whose spectral width is narrow, the PSD of $i(t)$ can be approximated as having a rectangular shape [11]-[13]. Thus, the PSD and autocorrelation of $i_C(t)$ can be approximated as

$$S_{i_C}(\omega) \approx S_I P_{\omega_{ch}/2}(\omega) \tag{22}$$

and

$$R_{i_C}(\tau) \approx S_I \frac{\sin(\omega_{ch}\tau/2)}{\pi\tau}, \tag{23}$$

respectively, where S_I denotes the single-sided PSD of $i(t)$, and $i_S(t)$ has identical statistics to $i_C(t)$.

The output of the LPF, $i_3(t)$, can be simplified to

$$i_3(t) = i_\phi(t) * h_L(\tau) \tag{24}$$

where

$$\begin{aligned} i_\phi(t) \triangleq i_C(t)\phi(t)\sin(\omega_{ch}t+\theta_i) \\ + i_S(t)\phi(t)\cos(\omega_{ch}t+\theta_i). \end{aligned} \tag{25}$$

In arriving (24), we assumed that the LPF provides sufficient attenuation to both the adjacent channel signals and the double frequency terms after the multiplier. Since $i_C(t)$, $i_S(t)$, and $\phi(t)$ are all independent, the autocorrelation function and PSD of $i_\phi(t)$ is given by

$$R_{i_\phi}(\tau) = R_\phi(\tau) R_{i_C}(\tau)\cos\omega_{ch}\tau \tag{26}$$

and

$$S_{i_\phi}(\omega) = S_\phi(\omega) * S_{i_C}(\omega) * \pi\left[\delta(\omega-\omega_{ch})+\delta(\omega+\omega_{ch})\right]. \tag{27}$$

Using (15) and (22), we have

$$\begin{aligned} S_\phi(\omega) * S_{i_C}(\omega) = \frac{\eta_{VCO}K_V^2 S_I}{8\pi\omega_0}\left[V(\omega+\omega_{ch}/2)\right. \\ \left. - V(\omega-\omega_{ch}/2) - W(\omega+\omega_{ch}/2) + W(\omega-\omega_{ch}/2)\right]. \end{aligned} \tag{28}$$

Then, using (17) and (28) in (27),

$$\begin{aligned} S_{i_\phi}(\omega) = \frac{\pi\mathfrak{L}(f)f^2 S_I}{2\omega_0}\left[V(\omega-\omega_{ch}/2) - V(\omega-3\omega_{ch}/2)\right. \\ + V(\omega+3\omega_{ch}/2) - V(\omega+\omega_{ch}/2) - W(\omega-\omega_{ch}/2) \\ \left. + W(\omega-3\omega_{ch}/2) - W(\omega+3\omega_{ch}/2) + W(\omega+\omega_{ch}/2)\right]. \end{aligned} \tag{29}$$

From (24), the autocorrelation function and PSD of $i_3(t)$ are given by

$$R_{i_3}(\tau) = R_{i_\phi}(\tau) * h_L(\tau) * h_L^*(-\tau) \tag{30}$$

and

$$S_{i_3}(\omega) = S_{i_\phi}(\omega)\,|H_L(\omega)|^2, \tag{31}$$

respectively, where $H_L(\omega)$ denotes the Fourier transform of $h_L(t)$.

Since the leakage signal coming from a nearby WiMAX MT is an unmodulated tone, the bandwidth of the LPF can be much smaller than ω_{ch}. Therefore, it is assumed that $S_{i_\phi}(\omega)$ is almost constant within the bandwidth of the LPF, and so can be approximated as

$$S_{i_3}(\omega) \approx S_{i_\phi}(0)\,|H_L(\omega)|^2, \tag{32}$$

yielding

$$\begin{aligned} S_{i_3}(\omega) \approx \frac{\pi\mathfrak{L}(f)f^2 S_I}{\omega_0}\left[V(3\omega_{ch}/2) - V(\omega_{ch}/2)\right. \\ \left. + W(\omega_{ch}/2) - W(3\omega_{ch}/2)\right]|H_L(\omega)|^2. \end{aligned} \tag{33}$$

$R_{i_3}(\tau)$ can be derived by the inverse Fourier transform of (33). With the ideal brick-wall frequency response of the LPF, $R_{i_3}(\tau)$ is given by

$$\begin{aligned} R_{i_3}(\tau) = \frac{\mathfrak{L}(f)f^2 S_I \sin(\omega_L\tau)}{\tau\omega_0}\left[V(3\omega_{ch}/2) - V(\omega_{ch}/2)\right. \\ \left. + W(\omega_{ch}/2) - W(3\omega_{ch}/2)\right] \end{aligned} \tag{34}$$

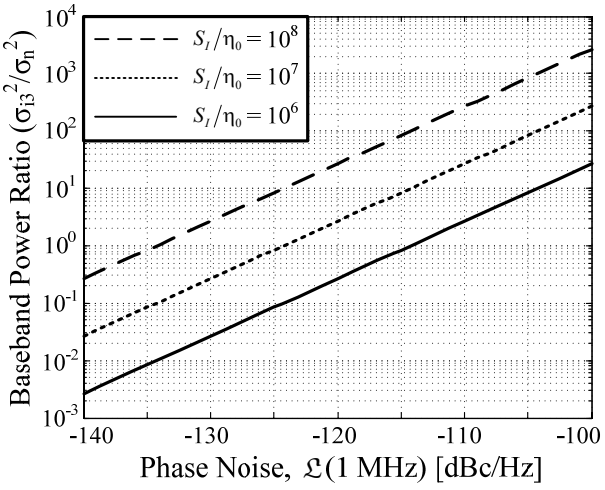

Figure 6. Baseband power ratio as a function of phase noise: $\omega_0 = 2\pi(10^5)$ rad/s, $\omega_{ch} = 10\pi(10^6)$ rad/s.

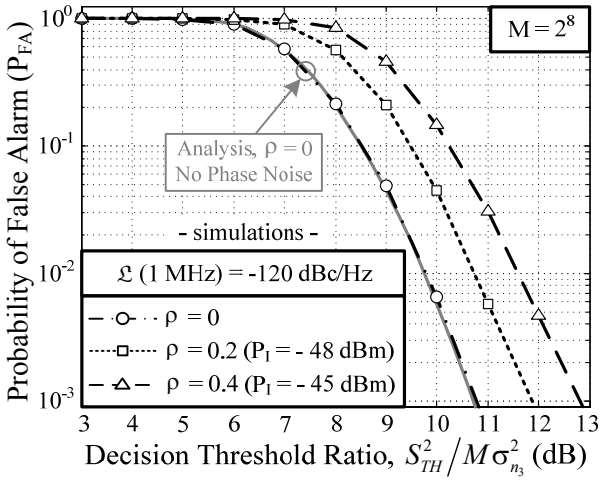

Figure 7. P_{FA} degradation due to the in-band interference. P_I denotes the power of $i(t)$: $\omega_0 = 2\pi(10^5)$ rad/s, $\omega_L = 2\pi(10^5)$ rad/s, and $\omega_{ch} = 10\pi(10^6)$ rad/s.

where ω_L denotes the bandwidth of the LPF. Therefore, the variance of $i_3(t)$ is given by

$$\sigma_{i_3}^2 = \frac{\mathfrak{L}(f) f^2 S_I \omega_L}{\omega_0}\Big[V(3\omega_{ch}/2) - V(\omega_{ch}/2) + W(\omega_{ch}/2) - W(3\omega_{ch}/2)\Big]. \quad (35)$$

The out-of-band signal, $i(t)$, interacts with the phase noise through the multiplier, and results an in-band interference, $i_3(t)$.

Denoting the variance of the baseband noise, when there is no phase noise, by σ_n^2, the ratio between the variance of the interference and σ_n^2 is given by

$$\rho = \frac{\sigma_{i_3}^2}{\sigma_n^2} = \frac{\pi\mathfrak{L}(f) f^2 S_I}{\eta_0\omega_0}\Big[V(3\omega_{ch}/2) - V(\omega_{ch}/2) + W(\omega_{ch}/2) - W(3\omega_{ch}/2)\Big]. \quad (36)$$

Figure 6 illustrates this ratio with different values of S_I/η_0. As the power of either $\phi(t)$ or $i(t)$ increases, the power of $i_3(t)$ becomes comparable to σ_n^2.

DETECTION PERFORMANCE DEGRADATION DUE TO PHASE NOISE

The spectrum broadening effect is now applied to the co-existence problem. When a WiMAX device receives only AWGN, the baseband signal is given by (7). However, since the phase noise of a typical VCO satisfies $|\phi(t)| \ll 1$ radian, the second term in the brackets on the right-hand side of (7) is negligible, and so

$$n_3(t) \approx n_A(t) * h_L(t). \quad (37)$$

Then, P_{FA} is given by [3]

$$P_{FA} = 1 - \left[1 - \exp\left(-\frac{S_{TH}^2}{M\sigma_{n_3}^2}\right)\right]^{\frac{M}{2}} \quad (38)$$

where S_{TH} denotes the pre-determined decision threshold.

The output of the LPF, when a strong interfering adjacent channel signal is present, should be modified to the sum of (24) and (37), given by

$$n_3(t) + i_3(t) = \left[n_A(t) + i_\phi(t)\right] * h_L(t). \quad (39)$$

Due to the in-band interference, $i_3(t)$, in (39), the DFT outputs experience increased variance, and so the magnitude responses are more likely to exceed S_{TH}. The effects of the phase noise on P_{FA} are shown in Figure 7.

If the leakage signal is present at the input, the detector performance is described by P_{MD}. Without a strong interfering adjacent channel signal, P_{MD} is given by [3]

$$P_{MD} = \left[1 - Q\left(\sqrt{M(SNR_{IN})}, \sqrt{\frac{2S_{TH}^2}{M\sigma_{n_3}^2}}\right)\right] \cdot \left[1 - \exp\left(-\frac{S_{TH}^2}{M\sigma_{n_3}^2}\right)\right]^{\frac{M}{2}-1} \quad (40)$$

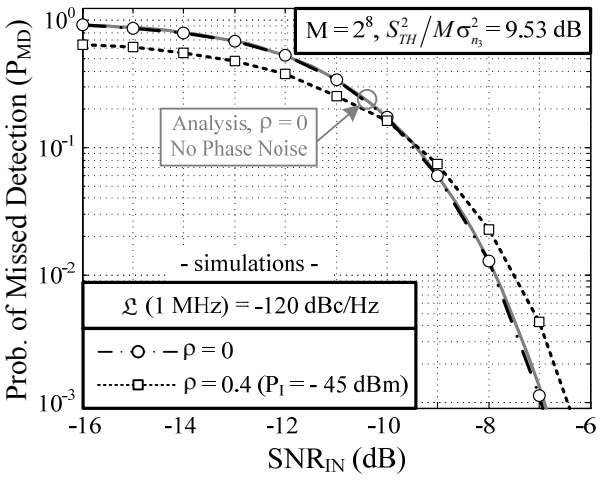

Figure 8. P_{MD} degradation due to the in-band interference. P_I denotes the power of $i(t)$: $\omega_0 = 2\pi(10^5)$ rad/s, $\omega_L = 2\pi(10^5)$ rad/s, and $\omega_{ch} = 10\pi(10^6)$ rad/s.

where $Q(x, y)$ is the Marcum Q-function, and SNR_{IN} denotes the input signal-to-noise ratio.

When a strong interfering signal is present, the P_{MD} response given by (40) must be affected. Figure 8 shows the P_{MD} responses with and without the phase noise interaction with an adjacent channel signal. It is noted that the P_{MD} curves in Figure 8 exhibit a crossover. At sufficiently high SNR, the DFT response to the leakage signal exceeds S_{TH} so that the in-band interference can only increase P_{MD}. However, at sufficiently low SNR, the DFT response to the leakage signal falls below S_{TH}, and thus the in-band interference can only lower P_{MD}.

CONCLUSION

In this paper, an analysis of the spectrum broadening effect due to the phase noise of a receiver LO signal is presented. It is shown that an adjacent channel signal interacts with the phase noise through a multiplier, and so the spectrum of the multiplier output broadens. As a result, an adjacent channel signal generates strong in-band interference in other channels, and thus degrades the performance. Since the front-end RF BPF cannot provide enough attenuation to the adjacent channel, the local oscillator has to be designed so that the phase noise has been sufficiently suppressed.

ACKNOWLEDGMENT

The authors would like to acknowledge the support of the UCSD Center for Wireless Communications, as well as the UC Discovery Grant Program.

REFERENCE

[1] FCC, "First report and order, revision of part 15 of the commission's rules regarding ultra-wideband transmission systems," ET Docket pp. 98-153, Feb. 2002.

[2] LAN / MAN standards committee of the IEEE computer society and the IEEE microwave theory and techniques society, "IEEE standard for local and metropolitan area networks – part 16: air interface for fixed broadband wireless access systems," IEEE Std. 802.16-2004, Revision of IEEE Std. 802.16-2001, Oct. 2004.

[3] S. Park, L. E. Larson, and L. B. Milstein, "Hidden mobile terminal device discovery in a UWB environment," in *IEEE Int. Conf. UWB*, Sep. 2006, pp. 417-421.

[4] R. S. Wolff, "An assessment of the potential terrestrial interference due to direct broadcast satellite television receivers," *IEEE J. Select. Areas Commun.*, vol. SAC-3, no. 1, pp. 148-154, Jan. 1985.

[5] J. G. Proakis, *Digital Communications*, 4th ed., McGraw-Hill, 2000.

[6] J. Lin, "A low-phase-noise 0.004-ppm/step DCXO with guaranteed monotonicity in the 90-nm CMOS process," *IEEE J. Solid-State Circuits*, vol. 40, no. 12, pp. 2726-2734, Dec. 2005.

[7] S. Farahvash, C. Quek, and M. Mak, "A temperature-compensated digitally-controlled crystal pierce oscillator for wireless applications," in *IEEE Int. Solid-State Circuits Conf. Dig. Tech. Papers*, Feb. 2008, pp. 352-619.

[8] T. H. Lee, *The Design of CMOS Radio-Frequency Integrated Circuits*, 2nd ed., Cambridge, 2004.

[9] A. Demir, "Computing timing jitter from phase noise spectra for oscillators and phase-locked loops with white and 1/f noise," *IEEE Trans. Circuits Syst. I. Regular Papers*, vol 53, no. 9, pp. 1869-1884, Sep. 2006.

[10] A. A. Abidi, "Phase Noise and Jitter in CMOS Ring Oscillators," *IEEE J. Solid-State Circuits*, vol. 41, no. 8, pp. 1803-1816, Aug. 2006.

[11] H. Ochiai and H. Imai, "On the distribution of the peak-to-average power ratio in OFDM signals," *IEEE Trans. Commun.*, vol. 49, no. 2, pp. 282-289, Feb. 2001.

[12] S. Wei, D. L. Goeckel, and P. E. Kelly, "A modern extreme value theory approach to calculating the

distribution of the peak-to-average power ratio in OFDM systems," in *IEEE Int. Conf. Commun.*, April 2002, pp. 1686-1690.

[13] A. G. Mason, G. M. Drury, and N. K. Lodge, "Digital television to the home – when will it come?," in *Int. Broadcasting Convention*, Sep. 1990, pp. 51-57.